Available online at www.sciencedirect.com
SCIENCE DIRECT®
Journal of Physics and Chemistry of Solids 65 (2004) 1837–1842
JOURNAL OF PHYSICS AND CHEMISTRY OF SOLIDS
www.elsevier.com/locate/jpcs

Application of the NRL tight-binding method to the heavy elements Pb and Po

M. Lach-hab[a,*], B. Akdim[b], D.A. Papaconstantopoulos[a], M.J. Mehl[a], N. Bernstein[a]

[a]Center for Computational Materials Science, Naval Research Laboratory, Washington, DC 20375, USA
[b]Air Force Research Laboratory, Materials and Manufacturing Directorate, WPAFB, OH 45433-7702, USA

Received 18 February 2004; revised 23 May 2004; accepted 8 June 2004

Abstract

We have applied the NRL tight-binding (TB) method to study the mechanical and electronic properties of the heavy elements Pb and Po. The predicted properties include ground-state structure, electronic band structure and elastic moduli. Phonon-dispersion curves at $T=0$ K were also determined. As demonstrated in this paper, the results are in good agreement with the full potential linearized augmented plane wave calculations and the available experimental data. In addition, we performed molecular-dynamics simulations to obtain various temperature-dependent quantities of Pb such as the atomic mean-square displacement, Debye-Waller factor and thermal expansion coefficient. With our TB we have also calculated the vacancy formation energy of Pb. Finally, we report on the effects of spin–orbit coupling, through our TB scheme, on electronic structure and energetic properties.

Keywords: D. Elastic properties; D. Electronic structure; D. Equations-of-state; D. Mechanical properties; D. Phonons; D. Thermal expansion

1. Introduction

The tight-binding (TB) method plays a crucial role in materials modeling, since it lies between more expensive but very accurate ab initio methods and the empirical methods that describe the dynamics of atoms in a given system, omitting all the details of the electronic structure. The original work by Slater and Koster (SK) [1] on the TB method, designed to interpolate the electronic structure [2] results from first-principles methods, was driven by the lack of fast computers. Therefore, one may perceive that the availability of high performance computing and parallel algorithms would favor the use of first-principles schemes over the TB. However, the use of TB methods has grown even greater nowadays, since the concept of the original scheme has been taken one step further, that is, formulation of the total energy within the TB approach [3]. This extension has allowed us to treat large systems (order of 1000 atoms) more efficiently than methods such as the linearized augmented plane wave (LAPW) [4,5]. The NRL-TB method [6,7] has been applied successfully to a large number of elemental solids, which include all the transition metals [7], sp metals [8], semiconductors [9], semi-metals [10], and more recently the binary alloys FeAl, CuAu and SiC [11–13]. Many papers on this method have been published, covering a variety of predicted properties, such as mechanical, electronic, and phononic; as a result, a large database [14] of SK parameters has been developed. As part of extending this database, the present work illustrates the results obtained for lead (Pb) and polonium (Po) using LAPW and the NRL-TB methods. In this work we will not describe the NRL-TB methodology, since many papers have been published on this approach. The reader is referred to the references given in these papers [15–17]. Pb and Po are heavy metals known experimentally to have as their ground structures the face-centered cubic (FCC) and simple cubic (SC), respectively. They are also known to have large spin–orbit coupling. Note that Po is the only element in the periodic table known to crystallize in the SC structure. Furthermore, theoretical studies of the bulk properties for Po single crystal are still scarce.

* Corresponding author. Fax: +1 202 404 7546.
E-mail address: lachhab@dave.nrl.navy.mil (M. Lach-hab).

0022-3697/$ - see front matter © 2004 Elsevier Ltd. All rights reserved.
doi:10.1016/j.jpcs.2004.06.020

The objective of this study is to provide the bulk properties of the aforementioned materials, predicted through the NRL-TB scheme. In addition we make the resulting SK parameters available for use in conjunction with molecular dynamics simulations [18,19]. Through this method we demonstrate that our TB model can successfully be applied to the study of the dynamical and finite temperature properties of Pb. We tested our TB parameters by calculating the mean-square displacement, Debye-Waller factor and thermal expansion coefficient. Also we have investigated the spin–orbit coupling effects on the energetics and band structure following our procedure discussed in Ref. [23]. In the following, Section 2 gives the approach taken to construct the fitting database from the FP-LAPW method and the detailed TB calculations. Section 3 illustrates the results of our calculations accompanied with discussion. Finally, a summary of the present work is given in Section 4.

2. The method

In order to perform the TB fit, a first-principles database of eigenvalues and their corresponding total energies was constructed, consisting of LAPW calculations for Pb and Po in the FCC, body-centered cubic (BCC) and SC structures using 89, 55 and 35 uniformly distributed k-points in the irreducible Brillouin zone (BZ), respectively. In order to better obtain sufficient accuracy of the elastic constants and phonon frequencies of Pb we also included in the fitting database the values of C_{11}–C_{12}, C_{44} and phonon frequencies at the high symmetry point X. In the LAPW calculations the muffin-tin sphere radii for both Pb and for Po were taken to be 2.5 a.u. and a plane wave cut off $RK_{max}=9.5$ for the size of the secular equation was used. These calculations were carried out in a semi-relativistic approximation, so they do not include the spin–orbit coupling [24]. The Hedin–Lundqvist [25] prescription was followed in calculating the exchange and correlation energy. To assure convergence of the total energy, the 5d core states were included in the LAPW calculations as part of the valence bands (semi-core states). The database of energies prepared as described above was then used to perform the TB fit for Pb and Po, where a non-orthogonal Hamiltonian matrix of size 4×4 (one s and three p orbitals) was used. The d states were omitted in the TB calculations, since they occur far below the s states and are very narrow. Hence, the TB parameters of the NRL-TB scheme were reduced from 97 to 41. These parameters were determined by a non-linear squares fit to the LAPW results for an extended range of volumes in the FCC, BCC and SC structures with an rms error in the fit of 34 and 2 mRy, averaging over all lattice constants, for the bands and total energies, respectively.

This determination of the TB parameters did not take into account the spin–orbit coupling effect. To address this issue we included the spin–orbit coupling in the NRL-TB a posteriori. This was done by doubling the size of the Hamiltonian matrix and introducing the values of the parameters $\lambda_{Pb}=0.03119$ Ry and $\lambda_{Po}=0.05129$ Ry to describe the spin–orbit interaction for Pb and Po, respectively. More details of this technique can be found in Ref. [23]. The above values of the spin–orbit parameter were taken from Herman's atomic structure calculations [26].

3. Results and discussion

3.1. Lead (Pb)

As mentioned in Section 2, the TB fit included the FCC, BCC, and SC energies as well as the energies corresponding to C_{11}–C_{12}, C_{44} and the phonons at X. As shown in Fig. 1, we see that there is excellent agreement between the TB and first-principles curves for the FCC structure, and that all other structures, including hexagonal close-packed (HCP) and diamond, are above the FCC ground state. This comes as no surprise since we have fitted the FCC structure and obtained a very low rms error for the total energies. We have not performed any first-principles calculations for the output structures (HCP, diamond) but our findings show the HCP between FCC and BCC structures, as expected, and the diamond at much higher energy. While the SC structure does not fit well, it is still at a higher energy value, which should not cause any concern about the transferability of these parameters for molecular dynamics simulations. The predictions of the unfitted structures (HCP, diamond) demonstrate the transferability of our SK parameters from one structure to another. The symbols in this figure represent the first-principles calculations and the lines are the TB results without spin–orbit. When the spin–orbit interaction is included, a uniform downshift of the total energies for FCC, BCC and SC structures is observed, keeping the same structural order. This suggests that the spin–orbit coupling has a small effect on the structural properties for Pb.

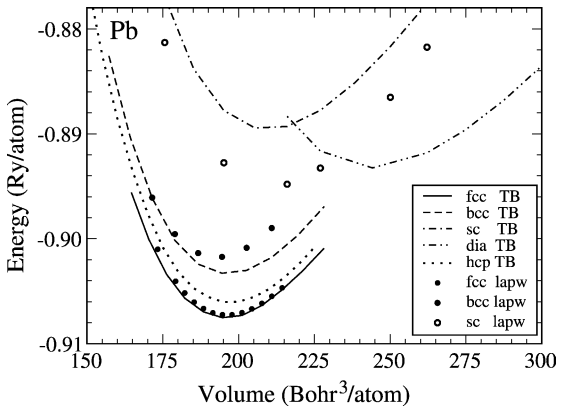

Fig. 1. Total energy vs volume for a number of crystal structures as well as the HCP and diamond structures for Pb (not included in the fit). The symbols represent the LAPW calculations, while the curves represent the TB results.

Table 1
Lattice constant (in a.u.) and elastic moduli of Pb (GPa)

	TB	TB (SO)	LAPW	Expt
a_0	9.22	9.26	9.22	9.35
B_0	50	43	54	45
C_{11}	63	54	63	50
C_{12}	44	37	50	42
C_{44}	23	21	22	15

Comparison is made between NRL-TB (with and without spin–orbit coupling), FP-LAPW, and to experimental data. SO, designates the calculations that include spin–orbit coupling.

Table 1 shows the equilibrium lattice constant, the elastic constants and the bulk modulus B_0 of Pb in the FCC structure, compared to first-principles LAPW calculations and to experiment. The elastic constants calculated by the NRL-TB as well as LAPW, although they satisfy the stability criteria [22] C_{11}–$C_{12}>0$ and $C_{44}>0$, are not in good quantitative agreement with experiment. All the calculations were performed at the equilibrium lattice constant. It should be noted from Table 1 that the inclusion of spin–orbit (as described in Ref. [23]) in the TB results gives a better agreement with experiment than the first-principles results in the determination of elastic constants.

In addition, we calculated the TB band structure at the experimental lattice constant $a=9.35$ Bohr. Fig. 2 displays the band structures, with (solid lines) and without spin–orbit (dashed lines) coupling, respectively. The effect of the spin–orbit interaction is notable in this case in the p-like bands above the Fermi energy (E_F), where the triply degenerate Γ_{15} state splits into Γ_6 and Γ_8, which are one- and two-fold degenerate, respectively. The only splitting that involves the valence band happens at W_3, which splits into W_6 and W_7. At X and L the spin–orbit interaction lifts the degeneracy only at states above the Fermi level. The states Γ_1, X_1, W_1, and L_1, which are s-like states, are not expected to be affected by the spin–orbit interaction. The band splitting is in good agreement with an early work of Loucks [27], which used the relativistic augmented plane wave method, and of Anderson and Gold [28], through an orthogonalized plane wave approach, where the pseudo-potential was fit to the experimental data. Such agreement suggests that the NRL-TB scheme is suitable for handling the effects of spin–orbit coupling, and could be extended to treat more complex materials, such as those with f state orbitals. In Fig. 3, we have plotted the total and decomposed DOS of Pb using NRL-TB method when spin–orbit is included (solid lines) and ignored (dashed lines). The inclusion of the spin–orbit interaction has a small effect on the p component of the total DOS. We note that no information regarding the angular momentum character was included during the performance of the fit, indicating the capability of this method to provide reliable eigenvectors. As is shown in Fig. 3, the broad peak, spanning energies between -1.0 and -0.6 Ry, is almost entirely due to s-like states, separated with a gap from the second peak that represents p-like states. These results suggest that no hybridization occurs between s and p states for this material.

We also computed the phonon spectrum along the high-symmetry directions of the BZ of the FCC lattice using the frozen phonon method [29,30]. In this method we create a supercell, where atoms are displaced from their equilibrium positions according to a specified polarization direction and the phase of this wave at the atomic position. The normal mode polarizations and frequencies are determined from the curvature of the energy as a function of the wave amplitude and a diagonalization of the dynamical matrix at each point in the BZ. In Table 2 we compare the phonon frequencies at high symmetry points from our TB model and experiment [20]. Although only the phonon frequencies at the point X were included in the fitting database, all other frequencies are also reproduced with fairly good accuracy. The phonon-dispersion curves along high-symmetry directions for Pb at

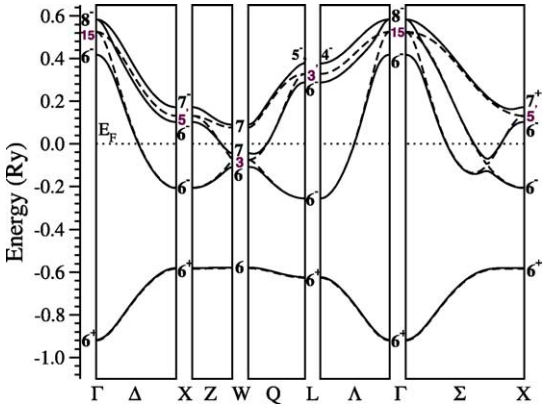

Fig. 2. Band structure of Pb at the experimental lattice constant 9.35 Bohr. The band structure is along high-symmetry directions in the Brillouin zone for FCC structure. The energies of the eigenstates have been uniformly shifted to set the Fermi level to zero. The solid lines show the calculations from the TB model with spin–orbit coupling included, and the dashed lines are the result from TB without spin–orbit.

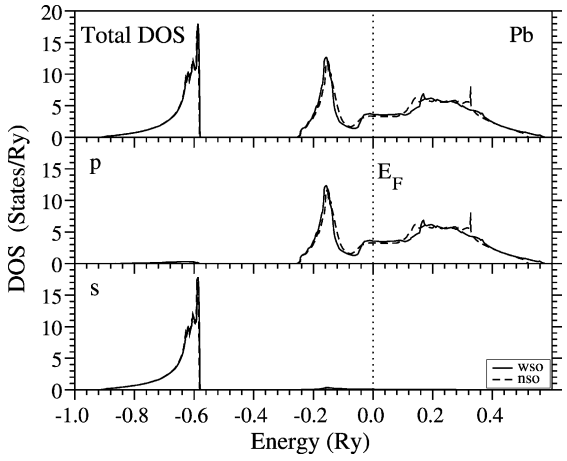

Fig. 3. Total and partial densities of states for FCC Pb at experimental lattice constant 9.35 Bohr. The solid and dashed lines depict the TB with spin–orbit and TB without results, respectively.

Table 2
Selected phonon frequencies (in cm^{-1}) computed with TB at high symmetry points in the Brillouin zone

	X_3	X_5	L_2	i_3	W_2	W_5
TB	60	40	67	37	52	50
Exp	62	30	73	30	57	46

The TB values are compared with experimental data [20].

$T=0$ K are shown in Fig. 4, together with experimental data [20]. The overall structure of the dispersion curves is well reproduced. The low-frequency transverse modes are overestimated compared to experiment while the longitudinal higher-frequency modes are mostly underestimated. We note that first-principles calculations of the phonon spectra have similar discrepancies with experiment [21].

In addition we used these parameters to perform molecular-dynamics (MD) simulations at various temperatures [18,19] on an FCC supercell containing 343 atoms, to obtain the temperature dependence of the atomic mean-square displacement, Debye-Waller factor and thermal expansion coefficient. The equations of motion were integrated using a time step of 2 fs for 2000 steps for the following temperatures: 150, 300, 450, 600 and 900 K. Then, by computing the mean-squared deviation of the atomic position averaging over all atoms and time steps, we derive the Debye-Waller factor for each temperature. Fig. 5 shows the Debye-Waller factor as a function of temperature compared to available experimental values [31]. As shown in the figure, the slope from TB is smaller than experiment but overall the results are reasonable, although not perfect.

To determine the thermal expansion coefficient α we calculate pressure as a function of temperature for a fixed volume using the trajectories from the previous simulations. For each temperature we selected all configurations from the trajectories generated by the MD and computed the pressure. From Fig. 6 we can see that the pressure as a function of temperature is perfectly linear. So by using

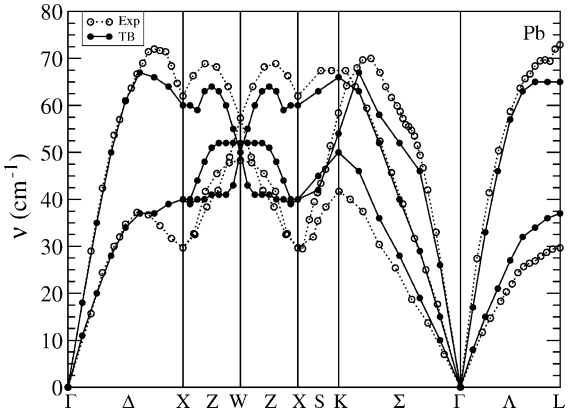

Fig. 4. Phonon frequencies for Pb (fcc) computed using the NRL-TB method (solid symbols) compared to experimental data [20] (open symbols).

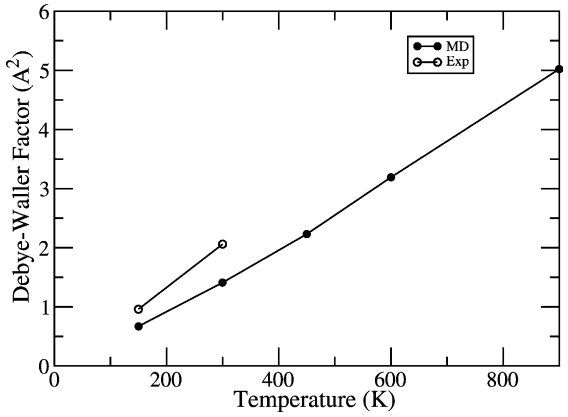

Fig. 5. Debye-Waller factor of Pb during MD simulations as a function of temperature. Solid circles are the molecular-dynamics simulations using TB model which are compared to experimental values [31] (open circle).

the definition for thermal expansion coefficient:

$$\alpha = \frac{1}{3B}\left(\frac{\partial P}{\partial T}\right)_V$$

where B is the bulk modulus taken at the experimental lattice constant, we get $\alpha = 2.6\times10^{-5}\,K^{-1}$. This value is found to be in agreement with the experimental [32] value of $2.9\times10^{-5}\,K^{-1}$ and other theoretical values [33].

For the calculation of the vacancy formation energy E_V^F we have used the expression:

$$E_V^F = E_V(N-1) - (N-1)\frac{E_0(N)}{N}$$

where $E_V(N-1)$ and $E_0(N)$ are the total energy of the supercell with and without the vacancy present as a function of the number of atoms N. We have computed the vacancy formation energy using the supercell total energy method [34] with a supercell of $N=125$ atoms. The conjugate gradient scheme was used to relax the atoms. At first we did not allow the atoms close to the vacancy to relax, and the value obtained for the unrelaxed formation energy was found to be 0.736 eV. When we allowed the atoms to relax

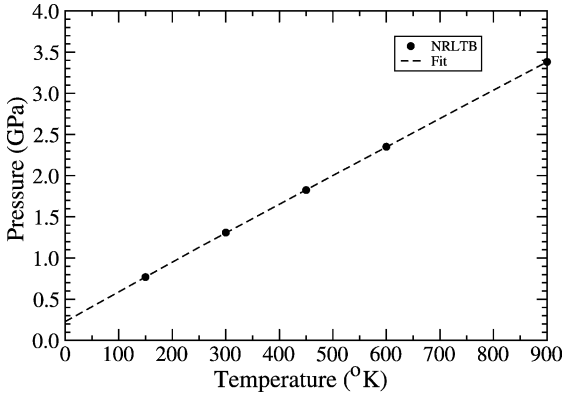

Fig. 6. Pressure as a function of temperature during TBMD simulations. The filled circles are the results of molecular-dynamics simulations using TB model; the line is the fit.

Table 3
Lattice constant (in a.u.) and elastic moduli of Po (GPa)

	TB	TB (SO)	LAPW	Expt
a_0	6.16	6.21	6.31	6.31
B_0	59	51	44	26
C_{11}	138	121	92	–
C_{12}	20	16	20	–
C_{44}	2	2	5	–

Comparison is made between NRL-TB (with and without spin–orbit coupling), FP-LAPW, and to experiment data. SO, designates the calculations that include spin–orbit coupling.

in the second calculation the relaxed formation energy is found to be 0.635 eV. The results are in good agreement with the experimental [35] formation energy of 0.54 eV.

3.2. Polonium (Po)

The TB fit for Po was performed using the LAPW results for FCC, BCC and SC structures. The resulting rms errors, averaged over 33 of the fitted lattice constants, are found to be about 29 and 2 mRy in the bands and total energies, respectively.

The calculated TB bulk properties of Po are in agreement with FP-LAPW results as shown in Table 3. The agreement of the bulk modulus B_0 and the equilibrium lattice parameter a_0 is expected, since the SC was included in the fit, but the challenge of the NRL-TB method is in the calculations of the shear moduli C_{11}, C_{12}, and C_{44}, which are found to be in good agreement with the LAPW results, considering the softness of the material. The inclusion of the spin–orbit changes the equilibrium lattice parameter by less than 1% and hence changes the elastic constants. Fig. 7 depicts the phase diagram of Po as a function of volume for a range of structure. The TB model reproduces the LAPW results well for the FCC, BCC, and SC structures to which it was fit. In these calculations we obtained HCP and diamond structures as an output of the TB method, with an energy higher than

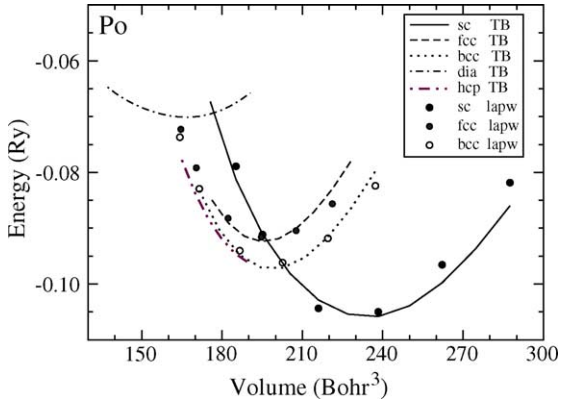

Fig. 7. Total energy vs volume for a number of crystal structures as well as the HCP and diamond structures for Po (not included in the fit). The symbols represent the LAPW calculations, while the curves represent the TB results.

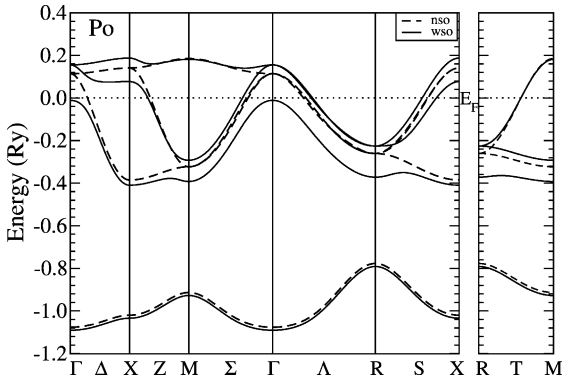

Fig. 8. Band structure of Po at the experimental lattice constant 6.31 Bohr. The band structure is along high-symmetry directions in the Brillouin zone for SC structure. The energies of the eigenstates have been uniformly shifted to set the Fermi level to zero. The solid lines show the calculations from TB model with spin–orbit coupling included, and the dashed lines are the result from TB without spin–orbit.

the ground structure (SC), as expected. It is particularly satisfying to find the position of HCP very near FCC. Similarly to Pb, a uniform total energy upshift has occurred, preserving the SC as the ground structure when spin–orbit coupling is included.

Fig. 8 shows the Po band structures, with (solid lines) and without the spin–orbit (dashed lines), respectively. We have used the SC lattice constant $a_0 = 6.31$ a.u., which was not part of the fitted database to demonstrate the transferability of our SK parameters in predicting the Po band structure. Just as in Pb, the effect of the spin–orbit coupling is evident by the band splitting in the p-like bands at high symmetry points, as expected. To our knowledge, no theoretical or experimental works are available to compare with in the Po case. However, on the basis of the good results obtained for Pb on band splitting, the Po TB results should be considered appropriate.

Fig. 9 shows good agreement of the total and decomposed DOS between NRL-TB when spin–orbit is (solid line) and is not (dashed line) included. Calculations were

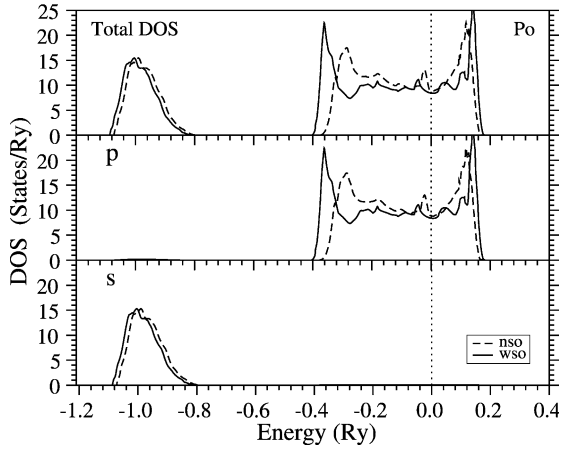

Fig. 9. Total and partial densities of states for SC Po at experimental lattice constant 6.31 Bohr. The solid and dashed lines depict the TB with spin–orbit and TB without results, respectively.

performed at $a_0 = 6.31$ a.u., in cubic lattice equilibrium. An examination of s and p DOS suggests that, as in Pb, no hybridization is taking place between s and p states for this material in its ground structure. This is evident from the decomposed DOS, which depicts the first and second peaks as 100% s-like and p-like states, respectively. Also, the inclusion of the spin–orbit does not affect the s–p hybridization, as suggested from the band structure calculation in Fig. 8.

4. Conclusions

In summary, the work presented in this paper shows that the NRL-TB scheme is successful in describing electronic and mechanical properties of the heavy metals Pb and Po. This was demonstrated by the agreement with the first-principles calculations and experimental results. The effect of spin–orbit coupling has also been investigated and found to be significant in the band structures results, but does not alter the structural properties. Moreover, the agreement of the Debye-Waller factor, thermal expansion coefficient and vacancy formation energy with experiment, in the case of Pb, shows the reliability of the parameters in studying the dynamical properties for finite temperatures.

Acknowledgements

This research was supported by the US Office of Naval Research. This work was also supported in part by a grant of HPC time from the DoD HPC Center, for computations on the IBM SP2 and SGI Origin at the Aeronautical Systems Center, Wright-Patterson Air Force Base, Dayton, OH.

References

[1] J.C. Slater, G.F. Koster, Phys. Rev. B 94 (1954) 1498.
[2] D.A. Papaconstantopoulos, Handbook of Electronic Structure of Elemental Solids, Plenum, New York, 1986.
[3] R.E. Cohen, M.J. Mehl, D.A. Papaconstantopoulos, Phys. Rev. B 50 (1994) 14694.
[4] O.K. Anderson, Phys. Rev. B 12 (1975) 3060.
[5] S.H. Wei, H. Krakauer, Phys. Rev. Lett. 55 (1985) 1200.
[6] M.J. Mehl, D.A. Papaconstantopoulos, Europhys. Lett. 31 (1995) 537.
[7] M.J. Mehl, D.A. Papaconstantopoulos, Phys. Rev. B 54 (1996) 4519.
[8] S.H. Yang, M.J. Mehl, D.A. Papaconstantopoulos, Phys. Rev. B 57 (1997) 2013.
[9] D.A. Papaconstantopoulos, M.J. Mehl, S.C. Erwin, M.R. Pederson, MRS Proceeding 491, Warrendale, PA 1998.
[10] B. Akdim, D.A. Papaconstantopoulos, M.J. Mehl, Phil. Mag. B 82 (2002) 47.
[11] S.H. Yang, M.J. Mehl, D.A. Papaconstantopoulos, M.B. Scott, J. Phys.: Condens. Matter 14 (2002) 1895.
[12] Ch.E. Lekka, N. Bernstein, M.J. Mehl, D.A. Papaconstantopoulos, Appl. Surf. Sci. 219 (2003) 158.
[13] N. Bernstein, H. Gotsis, D.A. Papaconstantopoulos, M.J. Mehl, Phys. Rev. B (submitted for publication).
[14] The TB parameters are available at http://cstd-www.nrl.navy.mil/bind/dostb.
[15] Tight-Binding Parametrization of First-Principles Results, Topics in Computational Materials Science, in: C.Y. Fong (Ed.),, World Scientific, Singapore, 1998, pp. 169–213. Ch. V, (Review Article).
[16] M.J. Mehl, D.A. Papaconstantopoulos, Phys. Rev. B 54 (1996) 4519.
[17] D.A. Papaconstantopoulos, M.J. Mehl, J. Phys.: Condens Matter 15 (2003) R413–R440.
[18] N. Bernstein, M.J. Mehl, D.A. Papaconstantopoulos, N.I. Papanicolaou, M.Z. Basant, E. Kaxiras, Phys. Rev. B 62 (2000) 4477.
[19] F. Kirchhoff, M.J. Mehl, N.I. Papanicolaou, D.A. Papaconstantopoulos, F.S. Khan, Phys. Rev. B 63 (2001) 195101.
[20] B.N. Brockhouse, T. Arase, G. Caglioti, K.R. Rao, A.D.B. Woods, Phys. Rev. 128 (1962) 1099.
[21] A.Y. Liu, A.A. Quong, Phys. Rev. B 53 (1996) R7575.
[22] M. Born, K. Huang, Dynamical Theory of Crystal Lattices, Clarendon, Oxford, 1956.
[23] M. Lach-hab, M. Keegan, D.A. Papaconstantopoulos, M.J. Mehl, J. Phys. Chem. Solid 61 (2000) 1639.
[24] D.D. Koelling, B.M. Harman, J. Phys. C 10 (1977) 3107.
[25] L. Hedin, B.L. Lundqvist, J. Phys. C: Solid State Phys. 4 (1971).
[26] F. Herman, S. Skillman, Atomic Structure Calcualtions, Prentice-Hall, Englewood Cliffs, NJ, 1963.
[27] T.L. Loucks, Phys. Rev. Lett. 14 (1965) 1072.
[28] J.R. Anderson, A.V. Gold, Phys. Rev. 139 (1965) A1459.
[29] K.M. Ho, C.L. Fu, B.N. Harmon, W. Weber, D.R. Hamann, Phys. Rev. Lett. 49 (1982) 673.
[30] S.W. Wei, M.Y. Chou, Phys. Rev. Lett. 69 (1992) 2799.
[31] L. Debye-Waller, M. Peng, G. Ren, S.L. Dudarev, M.J. Whelan, Acta Crystallogr., Sect. A: Found. Crystallogr. A52 (1996) 456.
[32] Weast, C. Robert (Eds.), CRC Handbook of Chemistry and Physics, CRC Press, Boca Raton, FL, 1987.
[33] R.A. MacDonald, W.M. MacDonald, Phys. Rev. B 24 (1981) 1715.
[34] M.J. Mehl, B.M. Klein, Physica B 172 (1991) 211.
[35] W. Triftshauser, Phys. Rev. B 12 (1975) 4634.